Nano Research

Open Access

Research Article

Regulation of graphdiyne-based nanozymes with enhanced oxidase-like activity by cobalt and nitrogen codoping

Jiali Liu[1,2,§], Xiaoli Wang[3,4,§], Yongfu Lian[2], Xue Wang[1,4], Xiuxiu Wang[1,4], Xingfa Gao[3] ✉, Baoyun Sun[1] ✉, and Xihong Guo[1] ✉

[1] *CAS Key Laboratory for Biomedical Effects of Nanomaterial & Nanosafety, Institute of High Energy Physics, Chinese Academy of Science, Beijing 100049, China*
[2] *Key Laboratory of Functional Inorganic Material Chemistry, Ministry of Education, School of Chemistry and Materials Science, Heilongjiang University, Harbin 150080, China*
[3] *Laboratory of Theoretical and Computational Nanoscience, National Center for Nanoscience and Technology, Beijing 100190, China*
[4] *University of Chinese Academy of Sciences, Beijing 100049, China*
§ *Jiali Liu and Xiaoli Wang contributed equally to this work.*

Cite this article: *Nano Research*, **2025**, *18*, 94907063. https://doi.org/10.26599/NR.2025.94907063

ABSTRACT: The development of nanozymes with excellent intrinsic oxidase-like activity and specificity has received increasing interest. Graphdiyne (GDY) could be a promising choice for designing nanozymes with enhanced oxidase (OXD)-like activity due to its unique structure and properties. Herein, Co-N-GDY with high OXD activity but no peroxidase (POD) activity was synthesized by codoping of cobalt (Co) and nitrogen (N) into GDY and compared with other GDY-based nanozymes (including GDY, Co-GDY, and N-GDY). Upon analyzing the doping effect of Co and N on the OXD-like and POD-like activities, we found that the combination of Co and N in GDY played a significant role in enhancing the OXD-like activity, and even reversed the POD-like activity of N-GDY to OXD-like activity of Co-N-GDY. The electrochemical experiment and the theoretical calculations provided an explanation for the mechanism and showed that the activity was closely linked to the reduction ability of O_2 or H_2O_2 on the nanozyme substrates, which was determined by the rate-determining step of the catalytic reaction.

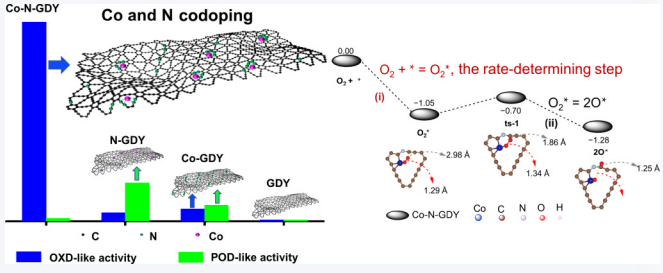

KEYWORDS: nanozymes, oxidase-like activity, graphdiyne, heteroatom doping, regulation

1 Introduction

Since the discovery of peroxidase (POD) mimic activity of Fe_3O_4 nanoparticles [1], nanomaterials with enzyme-like catalytic properties, named nanozymes, have attracted great attention due to their unique advantages such as high stability, easy large-scale production, and tunable structure and catalytic activity [2]. Till now, various nanomaterials have been developed to mimic the catalytic activity of natural enzymes, containing POD, oxidase (OXD), superoxide dismutase (SOD), and catalase (CAT), which are the most explored types of enzyme-like catalysis [3]. Typically, both POD and OXD are often used as pro-oxidant enzymes in many applications such as sensing, antitumor activity, antibacterial activity, and wastewater treatment [4]. Due to the destructive strong oxidizability and low stability of H_2O_2 as the substrate of POD, some attention of researchers is drawn to OXD-like nanozymes because of their efficient and selective utilization of oxygen.

However, nanozymes are less specific than natural enzymes, and they may exhibit multi-enzyme activities, such as OXD/POD-like [5, 6], OXD/POD/CAT-like [7, 8], OXD/POD/SOD-like [9], and even OXD/POD/CAT/SOD-like activities [10–12]. Although multiple enzyme-like activities can be utilized through cascade reactions in some fields, the selective reaction specificity of nanozymes is very important, since the lack of specificity may lead to the production of harmful byproducts during the reaction process [13]. Generally, the catalytic reactions of OXD and POD are enhanced under acidic conditions, while those of SOD and CAT are favored under neutral or alkaline conditions [14, 15]. Thus, the activity of OXD-like nanozymes can be regulated by the external environment such as pH to differentiate them from CAT- and SOD-like activities, but distinguishing them from POD-like activity may

Received: August 11, 2024; **Revised:** September 23, 2024
Accepted: October 2, 2024

✉Address correspondence to Xingfa Gao, gaoxf@nanoctr.cn; Baoyun Sun, sunby@ihep.ac.cn; Xihong Guo, guoxh@ihep.ac.cn

be more challenging. Hence, it is necessary to develop nanozymes with excellent intrinsic OXD-like specificity.

Graphdiyne (GDY), with large surface area, sp- and sp^2-hybrid carbon atoms, uniformly distributed pores, and excellent electronic conductivity, especially highly reactive acetylene units, could be a promising choice for designing nanozymes with enhanced OXD-like specificity. However, most of GDY-based nanozymes reported are peroxidase mimics [16–20]. Several strategies have been developed to improve the catalytic specificity of nanozymes, such as active site engineering, structure engineering, doping engineering, and surface modification [21]. Among them, heteroatom doping is an attractive strategy to enhance the activity and specificity of nanozymes due to its effectiveness, simplicity, and the wide variety of doping elements [22, 23]. For GDY-based nanozymes, heteroatoms such as N, B, O, and S have been used to improve their POD-like activity [24–26]. However, there is still a lack of research on the regulation of intrinsic OXD-like specificity of GDY-based nanozymes by heteroatom doping. Furthermore, the regulation mechanism of heteroatom doping on the enzyme catalytic reaction specificity is not very clear yet.

In this work, Co-N-GDY nanozyme with enhanced OXD-like activity was synthesized by codoping Co and N into GDY using melamine as N source and $CoCl_2{\cdot}6H_2O$ as Co source. The regulation effect of heteroatom doping on the OXD-like and POD-like activities of GDY-based nanozymes strategy was explored by comparing the OXD-like and POD-like activities between Co-N-GDY and other GDY-based nanozymes (GDY, Co-GDY, N-GDY, and Co/N-GDY). We found that the type of enzyme-like activities can be regulated by the different doping way and the GDY nanozyme with Co and N codoping into GDY showed the enhanced OXD-like activity and no POD-like activity, which was quite different from that of GDY doped with single element Co or N. Moreover, the regulation mechanism of Co and N doping in GDY was further explored through experimental measurements and theoretical calculations. This study will contribute to the rational design or adjustment of GDY-based nanozymes and further understanding of the regulation mechanism of heteroatom doping effect on the enzyme mimicking reactions.

2 Experimental

2.1 Materials

H_2O_2 (30%) and dimethyl sulfoxide (DMSO) were purchased from Beijing Chemicals, Inc. (Beijing, China). Hydrochloric acid, isopropanol (IPA), and ethanol absolute were purchased from Sinopharm Chemical Reagent Co., Ltd. Cobalt(II) chloride hexahydrate ($CoCl_2{\cdot}6H_2O$) was purchased from Shanghai Xian ding Biotechnology Co., Ltd. Melamine was purchased from Shanghai Macklin Biochemical Co., Ltd. 2,2'-Azinobis(3-ethylbenzothiazoline-6-sulfonic acid) diammonium salt (ABTS) was obtained from Huazhong Haiwei (Beijing) Gene Technology Co., Ltd. 3,3',5,5'-Tetramethylbenzidine (TMB) and o-phenylenediamine (OPD) were purchased from J&K Co., Ltd. (China). All reagents were used without further purification, and all aqueous solutions were prepared using ultrapure Millipore water (18.2 Ω).

2.2 Characterization

The ultraviolet–visible (UV–Vis) absorption spectra were measured by Agilent Cary 5000 spectrometer. The morphologies of the samples were characterized by scanning electron microscope (SEM, Hitachi S-4800), transmission electron microscope (TEM, JEM-2100F), and spherical aberration-corrected transmission electron microscopy (AC-TEM, ThermoFisher Scientific Themis Z). The X-ray absorption near-edge structure (XANES) at the Co K-edge was collected at Beijing Synchrotron Radiation Facility (BSRF) on the 1W1B beam line. X-ray photoelectron spectroscopy (XPS) was taken by Thermo Scientific K-Alpha. Raman spectrum was measured on Renishaw inVia plus. The X-ray diffractometer (XRD) pattern was obtained on Bruker D8 Advanced diffractometer. Fourier-transform infrared (FTIR) spectroscopy was obtained using Thermo Fisher iN10 spectrometer. The electrochemical measurements were performed on Shanghai Chenhua CHI760E workstation in a standard three-electrode cell. Cyclic voltammetry (CV) measurements were performed using a three-electrode system in acetate buffer. The platinum wire was used as the counter electrode and Ag/AgCl (saturated KCl) was used as the reference electrode. A nanozyme-modified glass-carbon (GC) electrode (3 mm diameter) was used as the working electrode. Electrochemical impedance spectroscopy (EIS) was performed in 5 mM $[Fe(CN)_6]^{3-/4-}$ containing 0.1 M KCl. The frequency range was between 0.01 Hz and 100 kHz, with a signal amplitude of 5 mV.

2.3 Synthesis of the GDY-based nanozymes

GDY was synthesized according to our previous work [27]. The pure GDY was obtained by using 1 M hydrochloric acid to remove the copper impurities. To realize the co-doping of Co and N, GDY and melamine (the mass ratio was 1:5 to ensure enough nitrogen source supply) were added into absolute ethanol. After the ultrasound for 30 min, $CoCl_2{\cdot}6H_2O$ was added into the solution and then stirred for 24 h at room temperature. The mass ratios of Co and GDY were 1.0:100. Then, the dried and ground sample was pretreated at 400 °C for 2 h, and then heated at a rate of 5 °C·min^{-1} to 900 °C for 1 h under Ar atmosphere. After the treatment with 1 M HCl at 80 °C for 2 h, the product (named Co-N-GDY) was obtained by water-washing and freeze-drying. For comparison, Co-GDY, N-GDY, and Co/N-GDY were also prepared under similar conditions of Co-N-GDY. Co-GDY was obtained without melamine and N-GDY was obtained without $CoCl_2{\cdot}6H_2O$, while Co/N-GDY was synthesized using the as-prepared N-GDY instead of GDY.

2.4 Enzymatic assays

To study the oxidase-like activity, 35 μL of GDY-based nanozymes aqueous solution (0.5 mg·mL^{-1}) was added as a catalyst to 940 μL of acetate buffer (0.1 M, pH = 4) solution containing 25 μL of TMB (25 mM in DMSO) solution. Then the mixed solution was incubated at room temperature for 10 min, and the absorbance was recorded at 652 nm by UV–Vis measurement. Unless otherwise specified, the experiments were carried out under air saturation. The effects of substrate type, catalyst concentration, pH value of acetate buffer solution, incubation temperature, and substrate TMB concentration on the oxidase-like activity were also investigated. To evaluate the catalytic activity of Co-N-GDY, TMB was used as the substrate for kinetic analysis. Michaelis constant (K_m) and the maximal reaction velocity (V_{max}) were obtained by Michaelis–Menten curve and the corresponding Lineweaver–Burk plot.

To investigate the peroxidase-like activity, 35 μL of GDY-based nanozymes aqueous solution (0.5 mg·mL^{-1}) was added as a catalyst to 915 μL of acetate buffer (0.1 M, pH 4) solution containing 25 μL of TMB solution (25 mM in DMSO) and 25 μL of H_2O_2 (0.2 M).

Then, the mixed solution was incubated in a spectrophotometer cell at room temperature for 10 min, and the absorbance was recorded at 652 nm for UV–Vis measurement. The peroxidase-like activities were measured under N_2-saturated solution to minimize the influence of dissolved oxygen as much as possible.

2.5 Computational details

All the calculations were performed by Vienna *ab initio* simulation package (VASP) [28, 29]. We used density functional thoery (DFT) + D2 method to describe and calculate all structures and the dispersion interactions [30, 31]. For the electronic structure of GDY-based nanozyme, we applied the Perdew–Burke–Ernzerhof (PBE) functional in all calculations [32]. For all structure optimizations, the cut-off energy is set at 500 eV and the convergence of the energy is endowed 10^{-5} eV with 0.02 eV·Å^{-1} of the force convergence. To prevent the interaction between layers, we applied 15 Å vacuum space along the vertical direction. We calculated 2 × 2 supercell with 3 × 3 × 1 Monkhorst–Pack *k*-points mesh sampling [33, 34]. For the transition states, we used the climbing image nudged elastic band (Cl-NEB) approach to search [35].

Additionally, the adsorption energy was calculated by the following Eq. (1)

$$\Delta E_{ads} = E_{(adsorbat/support)} - E_{(support)} - E_{(adsorbat)} \quad (1)$$

where $E_{(adsorbat/support)}$, $E_{(support)}$, and $E_{(adsorbat)}$ represented the total energies of the support with adsorbed molecule, the support, and the adsorbed molecule, respectively. Next, the formation energy of N-GDY was explained by Eq. (2)

$$\Delta E_f = E_{N\text{-}GDY} - E_{GDY} - 0.5E_{N2} + (E_{graphite}/n) \quad (2)$$

where $E_{N\text{-}GDY}$, E_{GDY}, E_{N2}, and $E_{graphite}$ were the total energies of N-GDY, GDY, N_2, and graphite, respectively. The n represented the quantity of N atoms, n = 1. Formation energy was negatively demonstrated the formation of N atom on the GDY was feasible.

The binding energy (ΔE_b) of Co-N-GDY was defined as follows (Eq. (3))

$$\Delta E_b = E_{(system)} - E_{(N\text{-}GDY)} - E_{(TM)} \quad (3)$$

where $E_{(system)}$, $E_{(N\text{-}GDY)}$, and $E_{(TM)}$ presented the total energies for system, N-doped graphdiyne, and isolated transition metals, respectively.

3 Results and discussion

3.1 Characterization of Co-N-GDY nanozyme

Co-N-GDY nanozyme was synthesized by codoping Co and N into GDY and characterized by various techniques. From the Raman spectra of prepared samples (Fig. S1(a) in the Electronic Supplementary Material (ESM)), two significant peaks at 1346 and 1592 cm^{-1} were observed, corresponding to the D band and G band of carbon nanomaterials, respectively. Since the successful doping of Co and N resulted in abundant structural defects on GDY [36], the I_D/I_G value of Co-N-GDY (I_D/I_G = 0.91) was significantly increased compared to GDY (I_D/I_G = 0.57). As to the characteristic peaks of alkynyl groups for GDY at 1944 and 2170 cm^{-1}, they decreased significantly after doping Co and N atoms, probably due to the destruction of some of the alkynyl groups of GDY during the pyrolysis and the incorporation [37]. From the XRD pattern, the peaks of Co-N-GDY were consistent with those of GDY (Fig. S1(b) in the ESM), corresponding to the (110) and (200) planes of carbon at around 23° and 43°, respectively. But no obvious crystal diffraction peaks of Co nanoparticles were observed in Co-N-GDY, indicating that the Co atoms were not clustered together. SEM and TEM revealed a lamellar structure with no visible nanoclusters or nanoparticles for Co-N-GDY (Figs. S2(a) and S2(b) in the ESM). Energy-dispersive X-ray (EDX) energy spectrum indicated the successful doping of Co and N into GDY (Fig. S2(c) in the ESM). Element mapping further proved Co and N elements were homogeneously distributed in carbon support (Fig. S2(d) in the ESM). AC-TEM was further carried out and indicated that the structure of Co in Co-N-GDY was highly dispersed (Fig. S2(e) in the ESM).

The presence state of Co and N, which plays a crucial role in the enzyme activity, is very important. Then XPS was adopted to further understand the compositions of Co-N-GDY. From the XPS survey spectrum of Co-N-GDY, an obvious N 1s peak and two weak Co 2p peaks were observed (Fig. S3 in the ESM). The peaks at 284.60 (C–C (sp^2)), 285.16 (C–C (sp)), 289.06 (C=O), 286.07 (C=N), and 286.89 eV (C–N) could be detected in the C 1s spectrum of Co-N-GDY (Fig. 1(a)) [38, 39]. The fitting high-resolution N 1s spectrum (Fig. 1(b)) displayed characteristic peaks located at 397.5 (sp-N), 398.5 (pyridinic N), 399.2 (Co–N), 399.9 (amino N), 401.2 (graphitic N), and 402.7 eV (oxidized N) [40, 41]. Both C 1s and N 1s results indicated the successful doping of N into GDY. Compared with the N 1s spectrum of N-GDY (Fig. S4 in the ESM), one of the most notable differences was the presence of Co–N bonds, which might be special active sites for nanozyme. The Co 2p spectrum displayed two characteristic peaks around 780.8 and 795.8 eV (Co $2p_{3/2}$ and Co $2p_{1/2}$) and two weak satellite peaks around 786.6 and 802.0 eV. However, the oxidation state of Co could not be clearly determined due to the weak intensity of the binding energy. The X-ray absorption spectroscopy (XAS) was used to further understand the electronic structure and local atomic coordination of the Co species. The XANES spectra of the Co K-edge of different samples containing Co were shown in Fig. 1(d), in which the spectral line of Co-N-GDY was very similar to that of the CoO and cobalt tetraphenylporphyrin (CoTPP) standard samples, indicating that the valence state of Co was close to Co^{2+}. Due to the better resolution in K and R spaces, the wavelet transforms (WT) of k^2-weighted extended X-ray absorption fine structure (EXAFS) were also provided (Figs. 1(e)–1(h)). The maximum peak at 4 Å^{-1} was observed for Co-N-GDY, which might be assigned to the Co–N coordination by comparing with Co foil, CoTPP, and CoO. The intensity maximum at 6 Å^{-1} corresponding to Co–Co coordination in Co foil could not be seen for Co-N-GDY, confirming that no Co particles existed in Co-N-GDY, which was consistent with the TEM results. The non-aggregated state is crucial for the optimal utilization of Co activity. In addition, the first-shell peak of EXAFS spectra for Co-N-GDY was fitted (Fig. S5 in the ESM), and the best fitting results indicated a mixed Co–N_2 and Co–N_3 (Table S1 in the ESM).

3.2 OXD-like behavior of Co-N-GDY nanozyme

The OXD-like activity of Co-N-GDY nanozyme was investigated using chromogenic substrates, including TMB, OPD, and ABTS (Fig. 2(a)). An obvious absorption peak at 652 nm was observed in the presence of Co-N-GDY, indicating that Co-N-GDY was active in catalyzing the oxidation of TMB. In addition, characteristic absorption peaks were also observed for OPD (~ 450 nm) and

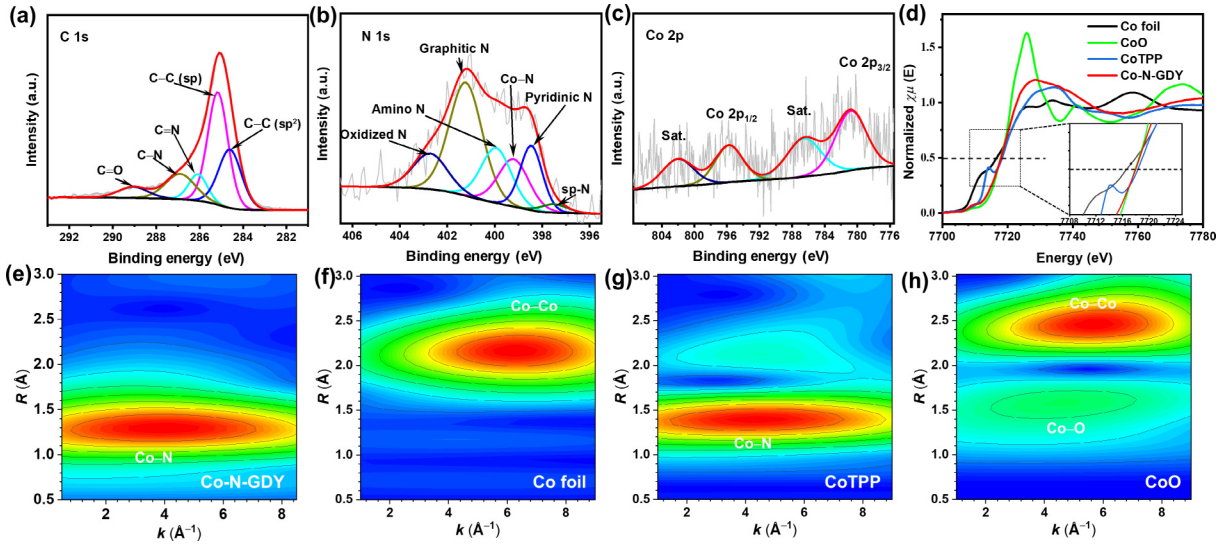

Figure 1 (a)–(c) High-resolution XPS spectra of C 1s, N 1s, and Co 2p of Co-N-GDY, respectively. (d) Co K-edge XANES spectra of Co Foil, CoO, CoTPP, and Co-N-GDY. WT for the k^2-weighted EXAFS signals of (e) Co-N-GDY, (f) Co foil, (g) CoTPP, and (h) CoO.

ABTS (~ 418 nm). These chromogenic reactions confirmed the intrinsic OXD-like activity of Co-N-GDY. The effects of pH, Co-N-GDY concentration, reaction time, and temperature on the activity of Co-N-GDY were also explored (Figs. S6(a)–S6(d) in the ESM). The absorbance at 652 nm initially increased with the increasing Co-N-GDY concentration and reaction time, but it gradually slowed down after reaching certain values. The catalytic activity of Co-N-GDY reached maximum absorbance at pH = 4 and approximately 25 °C. The mass ratio of Co and GDY (1.0:100) was obtained by comparing the OXD-like activities of GDY doping with Co and N at other mass ratio of Co and GDY to be (Fig. S6(e) in the ESM). To better evaluate the catalytic performance of Co-N-GDY, the kinetic parameters were determined through the Michaelis–Menten curve and the corresponding Lineweaver–Burk plot (Fig. S7 in the ESM). Michaelis constant and initial maximum velocity were obtained to be 0.27 mM and 15.66 × 10^{-8} M·s^{-1}, respectively. In addition, the catalytic activity of Co-N-GDY was also assessed by the K_w value, which is defined as the TMB oxidation rate catalyzed per unit mass concentration of the nanozyme catalyst. K_w was calculated to be 8.95 × 10^{-9} M·L·mg^{-1}·s^{-1}, which is higher than those of other materials. These parameters were listed and compared in Table S2 in the ESM. It was found that Co-N-GDY nanozyme exhibited good OXD-like activity.

The OXD-like activity of Co-N-GDY in air-, O_2-, and N_2-saturated solutions was then evaluated to further explore the reaction mechanism. After purging the solution with N_2, the absorbance value at 652 nm decreased to 6.6% of that under air, while the absorbance increased by 22.6% after bubbling pure O_2 into the solution (Fig. 2(b)). These results confirmed the OXD-like activity of Co-N-GDY was O_2-dependent, which may be derived from the catalytic ability of Co-N-GDY for activation of O_2 to generate reactive oxygen species. Free radical scavenging experiments were then carried out to further explore the reactive oxygen species generated in the reaction. As shown in Fig. 2(c), p-benzoquinone as a scavenger of superoxide radicals ($O_2^{\bullet-}$) significantly reduced the catalytic activity, while isopropanol ($^{\bullet}OH$ scavenger) had little effect on the reaction. In addition, L-tryptophan ($^1O_2$ scavenger) also had a certain effect on catalytic activity. Thus, it was concluded that the O_2 molecules were activated by Co-N-GDY to generate active oxygen intermediates ($O_2^{\bullet-}$ and $^1O_2$), and then the TMB was oxidized to ox-TMB by the strong oxidation of reactive oxygen species.

3.3 The influence of Co and N doping on the enzyme activity

In addition to Co-N-GDY, other GDY-based nanozymes (including GDY, Co-GDY, and N-GDY) were also synthesized for comparison to explore the effects and the possible regulatory mechanism of Co- or N-doping in GDY on the enzyme activity. Absorption spectra of TMB with different GDY-based nanozymes

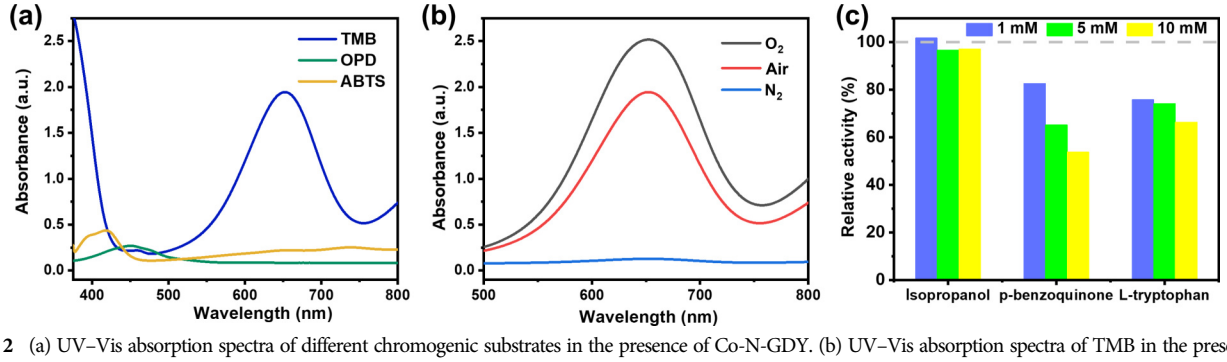

Figure 2 (a) UV–Vis absorption spectra of different chromogenic substrates in the presence of Co-N-GDY. (b) UV–Vis absorption spectra of TMB in the presence of Co-N-GDY under N_2-, air-, and O_2-saturated conditions. (c) The inhibition effects of different scavengers for TMB/Co-N-GDY system. Error bars represent the standard error of three measurements.

were measured. The OXD-like activity of pristine GDY was not observed since the characteristic absorption peak of ox-TMB didn't appear in the presence of GDY. Compared with GDY, the absorbance at 652 nm slightly increased upon the doping of Co or N (Fig. 3(a), inset). However, Co-GDY and N-GDY had much lower absorbance compared to Co-N-GDY, indicating the codoping of Co and N may play an important role in enhancing the catalytic activity. The sequence of OXD-like activity was Co-N-GDY > Co-GDY > N-GDY > GDY.

To further evaluate the regulatory effect of heteroatom doping on the enzyme activity, the POD-like activity was then investigated by employing TMB and H_2O_2 as the substrates (Fig. 3(b)). As Co-N-GDY had high OXD-like activity, the UV–Vis absorption spectra for Co-N-GDY, Co-GDY, N-GDY, and GDY were then measured after purging the buffer solution with N_2 for at least 20 min and incubating with the catalyst for 10 min under N_2-saturated solution, which was expected to minimize the influence of dissolved oxygen as much as possible. As seen from Fig. 3(b), no characteristic peak was observed for GDY, indicating that it couldn't catalyze H_2O_2 to oxide TMB. The characteristic peaks of ox-TMB were observed for Co-GDY or N-GDY, indicating the enhancement of the POD activity after heteroatoms doping of Co or N. However, the characteristic peak of ox-TMB didn't appear after the codoping of Co and N in GDY, indicating that the Co-N-GDY enzyme with enhanced OXD activity had no POD activity. To make it much clearer, the absorbance values at 652 nm ($A_{652\ nm}$) in Figs. 3(a) and 3(b) were compared in Fig. 3(c). Different from the OXD-like activity, the sequence of POD-like activity was N-GDY > Co-GDY > Co-N-GDY ≈ GDY. It can be concluded that: 1) the pristine GDY had almost no OXD-like or POD-like activity; 2) the doping of Co could make the graphdiyne exhibit weak OXD-like and POD-like activity; 3) the doping of N could make the graphdiyne exhibit weak OXD-like and relative high POD-like activity; and 4) the codoping of Co and N could make the graphdiyne exhibit high OXD-like but no POD-like activity. Therefore, by adjusting the doping method, we obtained an oxidase mimic without peroxidase activity.

3.4 The role of Co and N doping on the enzymatic activity regulation

As seen from the above, the combination of Co and N may play a key role in enhancing the OXD-like activity and specificity. Nitrogen can provide a large number of active sites for the growth of metal nanoparticles to increase the doping content of metal Co and enhance the catalytic performance. Thus, inductively coupled plasma optical emission spectroscopy (ICP-MS) was carried out and found that the Co content in Co-N-GDY and Co-GDY was 0.25 wt.% and 0.05 wt.%, respectively. However, although the Co content in Co-N-GDY was determined to be about 5 times that in Co-GDY, the absorbance of Co-N-GDY was more than 19 times that of Co-GDY when the concentration of nanozymes was controlled at 17.5 μg·mL^{-1} (Fig. 3(a)), indicating that the increase of Co content in Co-N-GDY might not be the main reason for the significant enhancement of its OXD-like activity. To better understand the role of doping Co, we then compared the absorbance of TMB in the presence of Co-GDY and Co-N-GDY under the same concentration of Co in the reaction systems according to the ICP-MS results. As seen from Fig. 4(a), the absorbance of ox-TMB for Co-N-GDY was much higher than that for Co-GDY at either Co concentration, further indicating that the enhancement of the OXD-like activity induced by Co content increase in Co-N-GDY was limited and the presence of N may play a very important role.

We then prepared Co/N-GDY using the as-prepared N-GDY instead of GDY under the same conditions of Co-N-GDY, that is, N was doped first and then Co was doped, which was beneficial to explore the influence of doping N. The UV–Vis absorption of TMB greatly increased in the presence of Co/N-GDY, and the absorbance of ox-TMB at 652 nm decreased significantly after purging the solution with N_2 for 20 min (Fig. 4(b)), which indicated that the Co/N-GDY exhibited the OXD-like activity. Moreover, the characteristic peaks of ox-TMB were not observed after adding H_2O_2 in the solution. Then, the OXD-like (air-saturated) and POD-like (N_2-saturated) activities of N-GDY and Co/N-GDY were compared. As shown in Fig. S8 in the ESM, the POD-like activity of N-GDY disappeared after the doping of Co (dash lines), and the good OXD-like activity of Co/N-GDY was observed (solid lines), demonstrating that the doping of Co greatly changed the enzyme mimic reaction of N-GDY. We thus inferred that the combination of Co and N in GDY was important for enhancing the performance of oxidase mimics, in which the presence of Co–N bond in Co-N-GDY had been verified by the above characterizations.

In order to understand the codoping effect of Co and N on the enhancement of the OXD-like activity, the electrocatalytic activities of GDY-based nanozymes toward the oxygen reduction reactions were explored by the CV test, since the OXD-like and oxygen reduction reaction (ORR) activities may follow a similar mechanism [10, 42]. Compared with the CV curves in the absence of oxygen, the reduction currents of electrodes modified with GDY-based nanozymes all increased with the injection of air in acetate buffers (pH = 4.0), i.e., increased with the increase of oxygen content (Figs. 5(a)–5(d)). The onset potential (E_{onset}) of oxygen reduction, defined as the intersection of the CV curves recorded in solutions with and without air (dashed lines in Fig. 5), was chosen

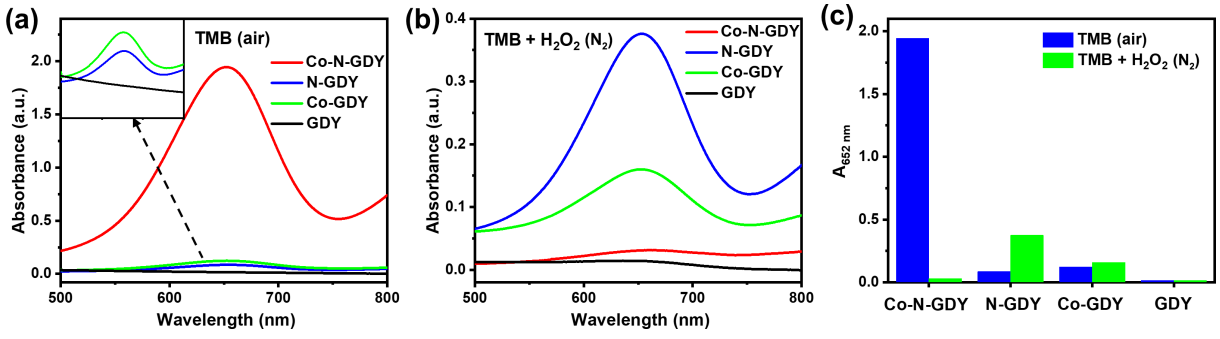

Figure 3 UV–Vis absorption spectra of (a) TMB (air-saturated solutions) and (b) TMB + H_2O_2 (N_2-saturated solutions) in the presence of different GDY-based nanozymes. (c) The absorbance values at 652 nm ($A_{652\ nm}$) in Figs. 3(a) and 3(b).

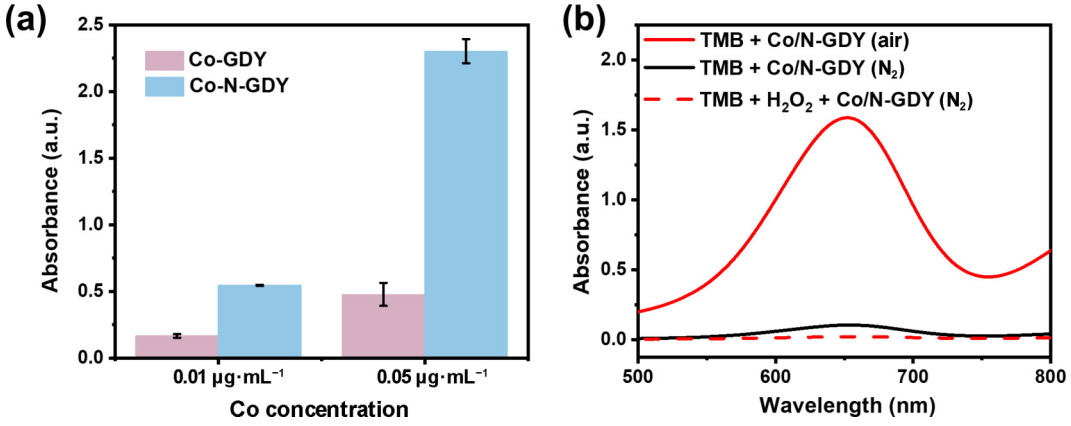

Figure 4 (a) Comparison of the absorbance at 652 nm between Co-GDY and Co-N-GDY by controlling the Co concentration in the system at the same level. Error bars represent the standard error of three measurements. (b) UV–Vis absorption spectra of TMB (air- and N_2-saturated solutions) and TMB + H_2O_2 (N_2-saturated solutions) in the presence of Co/N-GDY.

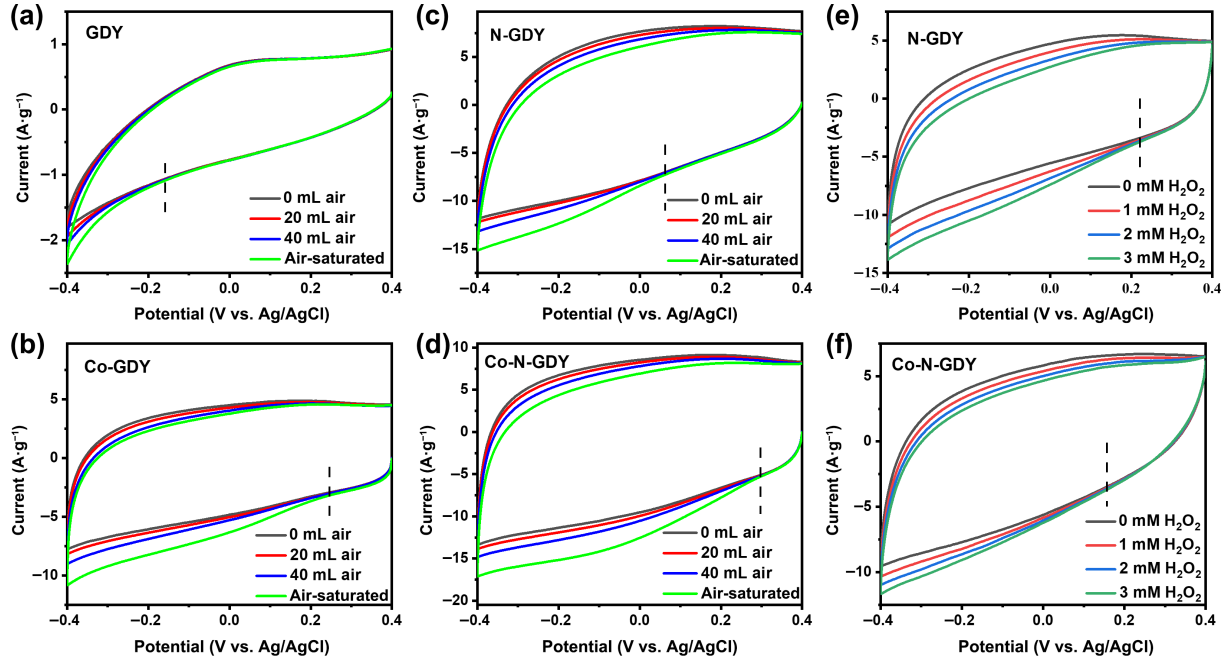

Figure 5 CV curves of (a) GDY, (b) Co-GDY, (c) N-GDY, and (d) Co-N-GDY modified electrodes at 0.1 V·s^{-1} in the acetate buffer (pH = 4.0) with and without air. CV curves of (e) N-GDY and (f) Co-N-GDY modified electrodes at 0.1 V·s^{-1} in the acetate buffer (pH = 4.0) with and without H_2O_2 (N_2-saturated).

as a descriptor to evaluate the catalytic activity, because E_{onset} is an effective indicator to evaluate electrocatalytic activity in the ORR [43, 44]. It could be seen that the E_{onset} shifted positively for doping GDYs in comparison with that of GDY. These indicated that the doping of Co or N could facilitate the oxygen reduction reaction. Moreover, the sequence of the E_{onset} of oxygen reduction was Co-N-GDY > Co-GDY > N-GDY > GDY, which was consistent with that for OXD-like activity determined above. The E_{onset} was the most positive for Co-N-GDY, indicating that oxygen was much more easily reduced on the surface of Co-N-GDY by codoping Co and N in GDY. Thus, it can be speculated that the codoping effect of Co and N on the enhancement of OXD-like activity of GDY may be due to the improved oxygen reactivity on the surface of Co-N-GDY. Considering the change between the POD-like activity of N-GDY and the OXD-like activity of Co-N-GDY, the electrocatalytic reaction of H_2O_2 was also compared for N-GDY and Co-N-GDY nanozymes modified electrodes (Figs. 5(e) and 5(f)). It had been found that the E_{onset} of O_2 reduction was much more positive than that of H_2O_2 reduction for Co-N-GDY, while it was the opposite for N-GDY. In addition, the E_{onset} of H_2O_2 reduction for N-GDY was more positive than that for Co-N-GDY. It meant that the reduction of H_2O_2 would be easier after the doping of N in GDY, but the reduction of O_2 turned to be much easier after the coupling of Co with N. These might further explain the reason why the POD-like activity of N-GDY disappeared after the doping of Co and exhibited OXD-like activity predominantly. In general, the reactivity of O_2 and H_2O_2 on the surface of nanozymes was changed through the doping regulation of Co and N in GDY, resulting in different OXD-like and POD-like behaviors of GDY-based nanozymes. Furthermore, the EIS Nyquist plots of GDY/GCE, Co-GDY/GCE, N-GDY/GCE, and Co-N-GDY/GCE were investigated and compared in Fig. S9 in the ESM. The sequence of the electron transfer resistance (R_{ct}) was Co-N-GDY (76.3 Ω) < Co-GDY (146.2 Ω) < N-GDY (189.6 Ω) < GDY (262.3 Ω). These results indicated Co-N-GDY had high electron transfer ability, which can promote the enzyme catalytic reaction.

To better understand the codoping effect of Co and N on the enzyme activity, the mechanisms of OXD and POD, especially the adsorption energy of the corresponding species, were designed and calculated theoretically for Co-N-GDY and N-GDY. The details of computational simulation methods can be found in the Experimental section. All possible structures were shown in Fig. S10 in the ESM. Considering the formation mechanism, N_{sp}-GDY model (doped with N) was selected based on the formation energy and Co-N'$_{sp}$-GDY model (doped with N and Co) was selected based on the binding energy (Fig. 6(a)).

For OXD activity, their mechanisms and energy curves were shown in Figs. 6(b) and 6(c). Normally, the activation of O_2 (the (i) process) was the key step in the reaction of oxidase [45]. As seen from Fig. 6(c), N_{sp}-GDY had weak adsorption of oxygen. It was difficult to adsorb O_2 ($\Delta E_{ads,\,O2}$ = 0.18 eV), with an activation energy barrier of 0.52 eV, which indicated that the catalytic reaction of O_2 did not easily occur on the surface of N-GDY. The adsorption of O_2 ($\Delta E_{ads,\,O2}$ = −1.05 eV) on the Co-N'$_{sp}$-GDY was a superoxygen structure (see Fig. S11 in the ESM), and that activation energy barrier was 0.35 eV. These results showed the catalytic reaction of O_2 was much more favorable on the surface of Co-N'$_{sp}$-GDY compared with N_{sp}-GDY, which explained the reason for the better OXD-like activity of Co-N-GDY. The complete reaction process and structure could be seen in Figs. S12 and S13 in the ESM.

Theoretical calculations of the peroxidase mechanism were also carried out for N_{sp}-GDY and Co-N'$_{sp}$-GDY according to the

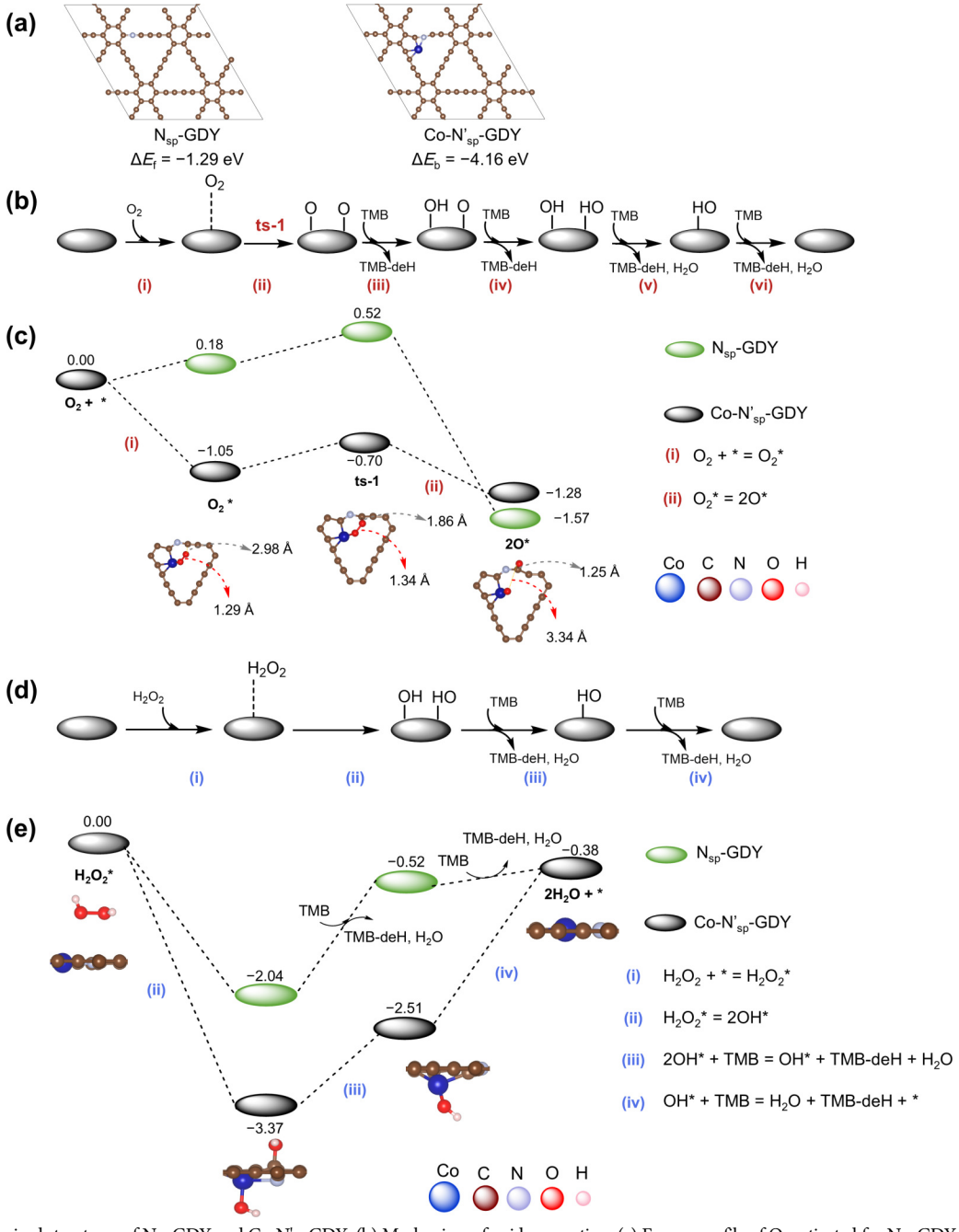

Figure 6 (a) Optimized structures of N_{sp}-GDY and Co-N'$_{sp}$-GDY. (b) Mechanism of oxidase reaction. (c) Energy profile of O_2 activated for N_{sp}-GDY and Co-N'$_{sp}$-GDY. (d) Mechanism of peroxidase reaction. (e) Energy profile of peroxidase for N_{sp}-GDY and Co-N'$_{sp}$-GDY.

peroxidase mechanism (Fig. 6(d)). Among them, the hydroxyl group formed by the (ii) process was adsorbed on the catalyst in the form of hetero-adsorption to overcome the deformation during catalytic adsorption. For Co-N'$_{sp}$-GDY system, the rate-determining step was the (iv) process that was OH* formed H_2O, with an energy barrier exceeding 2.13 eV. And the rate-determining step of N_{sp}-GDY system was the (iii) process that was 2OH* formed OH*, with an energy barrier exceeding 1.52 eV (Fig. 6(e)). In addition, Co-N'$_{sp}$-GDY had strong adsorption energy of OH ($\Delta E_{ads,\ 2OH}$ = −4.53 eV, $\Delta E_{ads,\ OH}$ = −2.14 eV, see Table S3 in the ESM), which made desorption more difficult than N_{sp}-GDY. Therefore, the peroxidase activity order is N_{sp}-GDY > Co-N'$_{sp}$-GDY. In summary, a better understanding of the regulation mechanism of Co and N doping in graphdiyne on the OXD-like and POD-like activities has been gained through theoretical calculations.

4 Conclusions

In summary, Co-N-GDY nanozyme with high oxidase-like but no peroxidase-like activity has been synthesized by the codoping of Co and N into GDY. Upon exploring the effect of Co and N doping on the enzyme activity, it was found that the combination of Co and N in GDY played a significant role in enhancing the OXD-like activity, while the single element Co or N doping in GDY cannot achieve it. In fact, the N-GDY with peroxidase activity reversed to oxidase-like enzyme activity upon further doping with Co. The electrochemical results and the theoretical calculations indicated that the activity of the nanozymes was closely associated with the O_2 or H_2O_2 reduction. Codoping of Co and N greatly enhanced the reduction reactivity of O_2 because of the more effective adsorption of O_2 on the surface of Co-N-GDY nanozyme, but the reduction of H_2O_2 was easier for N-GDY because of the lower energy barrier than that of Co-N-GDY. This work will contribute to the rational design or adjustment of GDY-based nanozymes and further understanding the structure–activity relationship.

Electronic Supplementary Material: Supplementary material (Raman spectra and XRD patterns of GDY and Co-N-GDY; SEM and TEM images, EDX energy spectrum, EDX mapping, and XPS survey spectrum of Co-N-GDY; N 1s spectra of Co-N-GDY and N-GDY; EXAFS fitting curve for Co-N-GDY; optimization of Co-N-GDY, reaction time, pH, and temperature; the Michaelis–Menten curve and the corresponding Lineweaver–Burk plot; OXD-like and POD-like activities of Co/N-GDY and N-GDY; Nyquist plots of GDY-based nanozymes; optimized structure of Co-N-GDY and N-GDY; structure of oxygen species; energy profile and reaction process of oxidase for Co-N-GDY and N-GDY; EXAFS fitting parameters; comparison of the kinetic parameters; adsorption energy of oxygen species) is available in the online version of this article at https://doi.org/10.26599/NR.2025.94907063.

Data availability

All data needed to support the conclusions in the paper are presented in the manuscript and the Electronic Supplementary Material. Additional data related to this paper may be requested from the corresponding author upon request.

Acknowledgements

This work was supported financially by the National Key Research and Development Program of China (Nos. 2022YFA1205900 and 2018YFA0703504), and the Directional Institutionalized Scientific Research Platform relied on Beijing Synchrotron Radiation Facility of Chinese Academy of Sciences. The authors wish to thank the facility's support of the 1W1B beamline of BSRF.

Declaration of competing interest

All the contributing authors report no conflict of interests in this work.

Author contribution statement

J. L. L.: Data curation, writing – original draft, investigation. X. L. W.: Formal analysis, writing – original draft. Y. F. L.: Formal analysis. X. W.: Formal analysis. X. X. W.: Formal analysis. X. F. G.: Conceptualization, writing – review & editing. B. Y. S.: Conceptualization, funding acquisition, writing – review & editing. X. H. G.: Conceptualization, project administration, writing – review & editing.

Use of AI statement

None.

References

[1] Gao, L. Z.; Zhuang, J.; Nie, L.; Zhang, J. B.; Zhang, Y.; Gu, N.; Wang, T. H.; Feng, J.; Yang, D. L.; Perrett, S. et al. Intrinsic peroxidase-like activity of ferromagnetic nanoparticles. *Nat. Nanotechnol.* **2007**, *2*, 577–583.

[2] Liang, M. M.; Yan, X. Y. Nanozymes: From new concepts, mechanisms, and standards to applications. *Acc. Chem. Res.* **2019**, *52*, 2190–2200.

[3] Wu, J. J. X.; Wang, X. Y.; Wang, Q.; Lou, Z. P.; Li, S. R.; Zhu, Y. Y.; Qin, L.; Wei, H. Nanomaterials with enzyme-like characteristics (nanozymes): Next-generation artificial enzymes (II). *Chem. Soc. Rev.* **2019**, *48*, 1004–1076.

[4] Su, L.; Qin, S. N.; Xie, Z. J.; Wang, L.; Khan, K.; Tareen, A. K.; Li, D. F.; Zhang, H. Multi-enzyme activity nanozymes for biosensing and disease treatment. *Coord. Chem. Rev.* **2022**, *473*, 214784.

[5] Wang, Y.; Chen, C.; Zhang, D. Sulfur-doping tuning oxygen vacancies in ultrathin 2D Ni–V mixed metal oxides for exceptional oxidase mimic and antibacterial applications. *J. Mater. Chem. C* **2021**, *9*, 15445–15451.

[6] Yang, K. L.; Xiu, W. J.; Li, Y. Q.; Wang, D.; Wen, Q. R.; Yuwen, L. H.; Li, X.; Yin, Z. W.; Liang, B.; Wang, L. H. NIR-responsive MoS_2–Cu_2WS_4 nanosheets for catalytic/photothermal therapy of methicillin-resistant *Staphylococcus aureus* infections. *Nanoscale* **2022**, *14*, 9796–9805.

[7] Zhang, T. T.; Liu, Y.; Pi, J. C.; Lu, N. N.; Zhang, R. S.; Chen, W. J.; Zhang, Z. Q.; Xing, D. M. A novel artificial peroxisome candidate based on nanozyme with excellent catalytic performance for biosensing. *Biosens. Bioelectron.* **2022**, *196*, 113686.

[8] Wu, S. L.; Wu, W. W.; Zhu, X. Y.; Li, M. H.; Zhao, J. G.; Dong, S. J. Atomically dispersed hierarchically ordered porous Fe–N–C single-atom nanozymes for dyes degradation. *Nano Res.* **2023**, *16*, 10840–10847.

[9] Huang, L.; Niu, Y. S.; Li, R. G.; Liu, H. Z.; Wang, Y.; Xu, G. F.; Li, Y.; Xu, Y. H. VO_x quantum dots with multienzyme-mimic activities and the application in constructing a three-dimensional (3D) coordinate system for accurate discrimination of the hydrogen peroxide over a broad concentration range. *Anal. Chem.* **2019**, *91*, 5753–5761.

[10] Fan, K. L.; Xi, J. Q.; Fan, L.; Wang, P. X.; Zhu, C. H.; Tang, Y.; Xu, X. D.; Liang, M. M.; Jiang, B.; Yan, X. Y. et al. *In vivo* guiding nitrogen-doped carbon nanozyme for tumor catalytic therapy. *Nat. Commun.* **2018**, *9*, 1440.

[11] Liu, X.; Yan, L.; Ren, H.; Cai, Y. Y.; Liu, C. Y.; Zeng, L. X.; Guo, J.; Liu, A. H. Facile synthesis of magnetic hierarchical flower-like Co_3O_4 spheres: Mechanism, excellent tetra-enzyme mimics and their colorimetric biosensing applications. *Biosens. Bioelectron.* **2020**, *165*, 112342.
[12] Liu, S.; Bai, Q.; Jiang, Y. J.; Gao, Y. H.; Chen, Z.; Shang, L. M.; Zhang, S. Y.; Yu, L. R.; Yang, D. Q.; Sui, N. et al. Multienzyme-like nanozyme encapsulated ocular microneedles for keratitis treatment. *Small* **2024**, *20*, 2308403.
[13] Fan, H. Z.; Zhang, R. F.; Fan, K. L.; Gao, L. Z.; Yan, X. Y. Exploring the specificity of nanozymes. *ACS Nano* **2024**, *18*, 2533–2540.
[14] Wang, Y.; Du, R. L.; Lee, L. Y. S.; Wong, K. Y. Rational design and structural engineering of heterogeneous single-atom nanozyme for biosensing. *Biosens. Bioelectron.* **2022**, *216*, 114662.
[15] Zhu, Y.; Yan, J.; Liu, J.; Chen, H. Y.; Gui, J. L.; Wu, C. Y.; Zhu, X. H.; Yin, P.; Liu, M. L.; Zhang, Y. Y. et al. Multi-mimic activities of Co_3O_4 nanopolyhedrons and application in regulating the content of intracellular hydrogen peroxide/oxygen. *ACS Appl. Nano Mater.* **2022**, *5*, 15102–15114.
[16] Ma, W. J.; Xue, Y. F.; Guo, S. Y.; Jiang, Y. N.; Wu, F.; Yu, P.; Mao, L. Q. Graphdiyne oxide: A new carbon nanozyme. *Chem. Commun.* **2020**, *56*, 5115–5118.
[17] Xu, C.; Ma, W. J.; Wang, H. Z.; Shao, L. H.; Li, W. Q.; Yu, P.; Mao, L. Q. Graphdiyne oxide substrate-enhanced peroxidase-mimicking performance of Ru nanoparticles with physiological pH preference. *Nano Res.* **2024**, *17*, 1123–1131.
[18] Zhu, Z. L.; Luo, H. Y.; Wang, T.; Zhang, C. H.; Liang, M. M.; Yang, D. Q.; Liu, M. H.; Yu, W. W.; Bai, Q.; Wang, L. N. et al. Plasmon-enhanced peroxidase-like activity of nitrogen-doped graphdiyne oxide quantum dots/gold-silver nanocage heterostructures for antimicrobial applications. *Chem. Mater.* **2022**, *34*, 1356–1368.
[19] Ahmed, S. R.; Cardoso, A. G.; Cobas, H. V.; Das, P.; Chen, A. C.; Srinivasan, S.; Rajabzadeh, A. R. Graphdiyne quantum dots for H_2O_2 and dopamine detection. *ACS Appl. Nano Mater.* **2023**, *6*, 8434–8443.
[20] Bai, Q.; Zhang, J. C.; Yu, Y. X.; Zhang, C. H.; Jiang, Y. J.; Yang, D. Q.; Liu, M. H.; Wang, L. N.; Du, F. L.; Sui, N. et al. Piezoelectric activatable nanozyme-based skin patch for rapid wound disinfection. *ACS Appl. Mater. Interfaces* **2022**, *14*, 26455–26468.
[21] Wei, G.; Liu, S. J.; Peng, Y. K.; Wei, H. On the specificity of nanozymes: A perspective. *Chin. J. Chem.* **2024**, *42*, 1515–1522.
[22] Zhang, S. F.; Ruan, H. Y.; Xin, Q.; Mu, X. Y.; Wang, H.; Zhang, X. D. Modulation of the biocatalytic activity and selectivity of CeO_2 nanozymes via atomic doping engineering. *Nanoscale* **2023**, *15*, 4408–4419.
[23] Xu, G. P.; Liu, K. H.; Jia, B. Q.; Dong, Z. Z.; Zhang, C. M.; Liu, X. D.; Qu, Y. Y.; Li, W. F.; Zhao, M. W.; Zhou, H. T. et al. Electron lock manipulates the catalytic selectivity of nanozyme. *ACS Nano* **2024**, *18*, 3814–3825.
[24] Bi, X. L.; Bai, Q.; Wang, L. N.; Du, F. L.; Liu, M. H.; Yu, W. W.; Li, S. H.; Li, J. Q.; Zhu, Z. L.; Sui, N. et al. Boron doped graphdiyne: A metal-free peroxidase mimetic nanozyme for antibacterial application. *Nano Res.* **2022**, *15*, 1446–1454.
[25] Zhang, C. H.; Chen, L.; Bai, Q.; Wang, L. N.; Li, S. H.; Sui, N.; Yang, D. Q.; Zhu, Z. L. Nonmetal graphdiyne nanozyme-based ferroptosis-apoptosis strategy for colon cancer therapy. *ACS Appl. Mater. Interfaces* **2022**, *14*, 27720–27732.
[26] Zhang, J. C.; Bai, Q.; Bi, X. L.; Zhang, C. H.; Shi, M. Y.; Yu, W. W.; Du, F. L.; Wang, L. N.; Wang, Z. B.; Zhu, Z. L. et al. Piezoelectric enhanced peroxidase-like activity of metal-free sulfur doped graphdiyne nanosheets for efficient water pollutant degradation and bacterial disinfection. *Nano Today* **2022**, *43*, 101429.
[27] Wang, D. M.; Liao, Y.; Yan, H. L.; Zhu, S.; Liu, Y. P.; Li, J.; Wang, X.; Guo, X. H.; Gu, Z. J.; Sun, B. Y. *In situ* formed Z-scheme graphdiyne heterojunction realizes NIR-photocatalytic oxygen evolution and selective radiosensitization for hypoxic tumors. *ACS Nano* **2022**, *16*, 21186–21198.
[28] Kresse, G.; Joubert, D. From ultrasoft pseudopotentials to the projector augmented-wave method. *Phys. Rev. B* **1999**, *59*, 1758–1775.
[29] Kresse, G.; Furthmüller, J. Efficient iterative schemes for *ab initio* total-energy calculations using a plane-wave basis set. *Phys. Rev. B* **1996**, *54*, 11169–11186.
[30] Grimme, S.; Antony, J.; Ehrlich, S.; Krieg, H. A consistent and accurate *ab initio* parametrization of density functional dispersion correction (DFT-D) for the 94 elements H–Pu. *J. Chem. Phys.* **2010**, *132*, 154104.
[31] Grimme, S.; Ehrlich, S.; Goerigk, L. Effect of the damping function in dispersion corrected density functional theory. *J. Comput. Chem.* **2011**, *32*, 1456–1465.
[32] Perdew, J. P.; Burke, K.; Ernzerhof, M. Generalized gradient approximation made simple. *Phys. Rev. Lett.* **1996**, *77*, 3865–3868.
[33] Monkhorst, H. J.; Pack, J. D. Special points for Brillouin-zone integrations. *Phys. Rev. B* **1976**, *13*, 5188–5192.
[34] Evarestov, R. A.; Smirnov, V. P. Modification of the Monkhorst-Pack special points meshes in the Brillouin zone for density functional theory and Hartree–Fock calculations. *Phys. Rev. B* **2004**, *70*, 233101.
[35] Henkelman, G.; Uberuaga, B. P.; Jónsson, H. A climbing image nudged elastic band method for finding saddle points and minimum energy paths. *J. Chem. Phys.* **2000**, *113*, 9901–9904.
[36] Wang, X.; Yang, Z.; Si, W.; Shen, X.; Li, X.; Li, R.; Lv, Q.; Wang, N.; Huang, C. Cobalt-nitrogen-doped graphdiyne as an efficient bifunctional catalyst for oxygen reduction and hydrogen evolution reactions. *Carbon* **2019**, *147*, 9–18.
[37] Wang, T.; Bai, Q.; Zhu, Z. L.; Xiao, H. L.; Jiang, F. Y.; Du, F. L.; Yu, W. W.; Liu, M. H.; Sui, N. Graphdiyne-supported palladium-iron nanosheets: A dual-functional peroxidase mimetic nanozyme for glutathione detection and antibacterial application. *Chem. Eng. J.* **2021**, *413*, 127537.
[38] Liu, R. J.; Liu, H. B.; Li, Y. L.; Yi, Y. P.; Shang, X. K.; Zhang, S. S.; Yu, X. L.; Zhang, S. J.; Cao, H. B.; Zhang, G. J. Nitrogen-doped graphdiyne as a metal-free catalyst for high-performance oxygen reduction reactions. *Nanoscale* **2014**, *6*, 11336–11343.
[39] Bao, H. H.; Wang, L.; Li, C.; Luo, J. Structural characterization and identification of graphdiyne and graphdiyne-based materials. *ACS Appl. Mater. Interfaces* **2019**, *11*, 2717–2729.
[40] Zhao, Y. S.; Wan, J. W.; Yao, H. Y.; Zhang, L. J.; Lin, K. F.; Wang, L.; Yang, N. L.; Liu, D. B.; Song, L.; Zhu, J. et al. Few-layer graphdiyne doped with sp-hybridized nitrogen atoms at acetylenic sites for oxygen reduction electrocatalysis. *Nat. Chem.* **2018**, *10*, 924–931.
[41] Zhang, C.; Zhang, H. K.; Wan, X.; Xie, Y.; Bentel, M. J.; Yu, Z. J.; Chen, Z. G.; He, J. A.; Li, J. L.; Xiang, X. Z. et al. Nitrogen-doped graphdiyne nanotubes for metal-free activation of peroxymonosulfate and enhanced degradation of recalcitrant heterocyclic contaminants. *ACS EST Engg.* **2023**, *3*, 969–980.
[42] Lu, X. Y.; Gao, S. S.; Lin, H.; Tian, H.; Xu, D. L.; Shi, J. L. Bridging oxidase catalysis and oxygen reduction electrocatalysis by model single-atom catalysts. *Natl. Sci. Rev.* **2022**, *9*, nwac022.
[43] Luo, M. C.; Koper, M. T. M. A kinetic descriptor for the electrolyte effect on the oxygen reduction kinetics on Pt(111). *Nat. Catal.* **2022**, *5*, 615–623.
[44] Batchelor-McAuley, C. Defining the onset potential. *Curr. Opin. Electrochem.* **2023**, *37*, 101176.
[45] Shen, X. M.; Wang, Z. Z.; Gao, X. J.; Gao, X. F. Reaction mechanisms and kinetics of nanozymes: Insights from theory and computation. *Adv. Mater.* **2024**, *36*, 2211151

This is an open access article under the terms of the Creative Commons Attribution 4.0 International License (CC BY 4.0, https://creativecommons.org/licenses/by/4.0/).

© The Author(s) 2025. Published by Tsinghua University Press.